React Engineering, Environmental, and Applied Sciences
https://research.federalpolyede.edu.ng/react-eeas
1(1), 22-43, (2025)
RESEARCH ARTICLE

Investigating the mechanical performance of Al-Mg-Si alloy for structural applications

Takalani Madzivhandila[1], Festus Ben[1,2]

[1] Centre for Nanoengineering and Advanced Materials, Department of Metallurgy, University of Johannesburg, Johannesburg, South Africa
[2] Centre for Advanced Materials Research and Development, Department of Physics, Federal Polytechnic Ede, Ede, Nigeria

Received: 25 December 2024 | *Accepted:* 12 February 2025 | *Published:* 02 March 2025
Corresponding author: festobit@gmail.com | Festus Ben

Abstract

Al-Mg-Si alloys offer lightweight properties and an excellent strength-to-weight ratio, making them attractive for engineering applications. However, limitations in their mechanical performance have driven interest in reinforcing these alloys with synthetic ceramics and agro-waste residues. Although previous studies have explored plantain peel ash, rice husk ash, and coconut shell ash, comprehensive investigations into cassava peel ash (CPA) and alumina-reinforced Al-Mg-Si alloys remain limited. This study examines the mechanistic performance of CPA/Alumina-reinforced Al-Mg-Si composites manufactured via a two-stage stir casting procedure, with CPA contents of 2–10 wt.%. Composites were evaluated for porosity, density, hardness, tensile and yield strength, ductility, E-modulus, toughness, strain at failure, and wear resistance. Microstructural analysis revealed heterogeneous, roundish reinforcement dispersion, with XRF and XRD confirming silica as the dominant oxide phase. The composites exhibited lightweight characteristics with porosity between 0.93–1.94%. Hardness ranged from 57.10 to 68.24 BHN, tensile strength from 95.35 MPa (CPA-10) to 210.68 MPa (CPA-4), and yield strength peaked at 175.09 MPa (CPA-4). CPA-0 showed the highest toughness (5.55 J) and ductility (12.22%), while wear resistance improved progressively with CPA, peaking at CPA-10 (1.280 mm/mm^3). CPA-4, with 4 wt.% CPA and 6 wt.% alumina, emerged as the optimal composition, offering an excellent balance of strength, stiffness, and moderate ductility. The findings confirm that cassava peel ash, when optimally hybridized with alumina, can serve as a sustainable, eco-friendly reinforcement, significantly enhancing the mechanical performance of aluminum alloys for broader structural and engineering applications.

Keywords Al-Mg-Si alloy, cassava peel ash, silica, mechanical performance, agro-waste residues, two-step stir casting

1. Introduction

Aluminum-Magnesium-Silicon (Al-Mg-Si) alloys are widely recognized for their high strength, excellent corrosion resistance, formability, and lightweight nature. As part of the 6xxx series, they are particularly valued in structural applications owing to their exceptional strength-to-weight performance, weldability, machinability, and thermal stability. The formation of intermetallic Mg_2Si phases enhances their mechanical strength through precipitation hardening [1], making them well-suited for extrusion processes with excellent heat-treatment properties [2]. These attributes have positioned Al-Mg-Si alloys as essential materials in various industries, including marine structures [3], transportation (aerospace and automotive) [4], electrical conductors [5], civil infrastructure [6], and additive manufacturing [7]. However, achieving resistance to spalling and cracking from rapid heating while maintaining structural integrity remains a challenge, particularly in the transportation sector. Consequently, research into optimizing these alloys continues to be a priority.

The mechanistic characteristics of Al-Mg-Si alloys can be significantly enhanced through reinforcement with particulate materials and appropriate heat treatment. Synthetic ceramic reinforcements (SCRs), including TiC, SiO_2, WC, Al_2O_3, SiC, and CNTs have demonstrated considerable improvements in hardness and strength due to their load-bearing and pinning effects within the alloy matrix [8,9]. For example, the incorporation of 10 wt%

Al_2O_3 in AA6063 increased hardness from 25 BHN (0 wt% Al_2O_3) to 74.70 BHN, Young's modulus from 11.35 GPa to 15.63 GPa, ductility from 3.14% to 12.11%, and strength from 118.87 MPa to 207.49 MPa [6,10]. The enhanced performance is attributed to improved mechanical interlocking and bonding between the matrix and reinforcements, as well as the temperature mismatch and high elastic modulus of Al_2O_3, which further strengthens the composite [11]. Similarly, hybrid reinforcements combining SiC and TiB_2 have been found to improve tensile, flexural, and impact strength, with SiC playing a dominant role in enhancing mechanical performance [12].

Despite the advantages of SCRs, their high production costs and environmental impact, particularly in terms of greenhouse gas emissions, pose significant challenges [13,14]. As a result, research has increasingly focused on sustainable and cost-effective reinforcement alternatives, such as agro-waste residues, which offer a viable replacement for conventional synthetic ceramics. Agro-waste residues, if not adequately managed, contribute to environmental pollution, making their repurposing a key area of interest in green engineering [15–17]. Studies have demonstrated that agro-waste-derived reinforcements can enhance the mechanistic properties of Al-Mg-Si alloys. For instance, rice husk ash particulates have shown good interfacial bonding with Al-Mg-Si matrices [18], while agro-waste-reinforced composites have exhibited improved hardness [19,20], ductility [21], and strength [22] due to efficient load transfer mechanisms. Extensive research presented in Table 1 on using agro-waste residues as reinforcements highlights their growing significance as sustainable materials for composite development.

Among the agro-waste residues listed in Table 1, cassava (*Manihot esculenta*) peels remain underexplored as a reinforcement material for Al-Mg-Si alloys. Cassava is abundantly cultivated in Sub-Saharan Africa, accounting for approximately 63.1% of global production [33], with Nigeria contributing more than 18% annually [34]. Its peels have been investigated for various applications, including pozzolanic material for partial cement replacement [35,36], electrode material for supercapacitors [37], and a biogas source when blended with animal waste [38]. Despite these promising prospects, limited studies have explored cassava peel ash (CPA) as a monolithic or hybrid reinforcement in Al-Mg-Si matrix composites. Utilizing cassava peels aligns with global sustainability goals, particularly in reducing carbon footprints and achieving net-zero emissions by 2030 [39].

The increasing emphasis on green manufacturing underscores the potential of cassava peel as a low-cost, eco-friendly reinforcement alternative for engineering applications. Previous research indicates that heat-treated CPA can enhance the structural and wear performance of AA6063-based composites fabricated using two-step stir casting [1,24]. For instance, Ben and Olubambi investigated only the tribological performance of CPA/Al_2O_3 reinforced AMCs without assessing their mechanistic behaviour [1]. Olaniran et al. investigated the influence of CPA/SiC particulates on Al-Mg-Si composites' tribological and physico-mechanical properties. Their study reported significant improvements compared to the unreinforced matrix but did not provide data on density, ductility, or Young's modulus (Table 1) [24].

Building on the prior investigations, this study aims to extend the understanding of Al-Mg-Si matrix composites by comprehensively evaluating their mechanistic performance when reinforced with agro-waste residues such as CPA and alumina. While previous research has explored their tribological and microstructural behavior, a significant gap exists in assessing how these reinforcements influence key mechanical properties, including Young's modulus, yield strength, tensile strength, ductility, toughness, and failure strain. These mechanistic properties, which are critical indicators of structural reliability, have not been concurrently assessed in the literature for CPA reinforced composites. This study addresses that gap by examining monolithic and hybrid reinforcements using a two-stage stir casting procedure, focusing on evaluating their performance under tensile, bending, and dynamic loading conditions.

A two-step stir casting procedure was adopted owing to its efficiency in ensuring uniform distribution of reinforcement phases throughout the matrix, thereby optimizing the structural characteristics of the composites [22,40,41]. The unique contribution of this research is its comprehensive evaluation of the physical and mechanical performance of the CPA-reinforced composites and the innovative use of cassava peel as a reinforcement material, repurposing agro-waste from an environmental pollutant into a sustainable engineering solution for advanced composite fabrication. The insights gained will contribute to developing sustainable, high-performance materials for structural components in transportation, construction, and other engineering sectors.

Table 1. Mechanistic properties of Al-Mg-Si matrix composites incorporating agro-waste reinforcements

Al series	Reinforcement types		Range Mechanistic performance					Ref.
	Agro-wastes	**SCRs**	**Hardness (BHN)**	**Tensile strength (MPa)**	**Young's Modulus (Gpa)**	**Ductility (%)**	**Density (g/cm^3)**	
Al6063	Bean pods	Al_2O_3	74.70 to 105.04	118.87 to 200.62	11.35 to 15.63	3.14 to 12.11	2.78 to 2.74	[6]
Al6061	Coconut shell	None	40.86 to 55.2	70.00 to 160.27	NR	NR	NR	[23]
Al-Mg-Si	Cassava peel	SiC	47.2 to 57.5	143.5 to 189.9	NR	NR	NR	[24]
Al6063	Manihot esculenta	Al_2O_3	74.70 to 107.47	NR	NR	NR	2.64 to 2.74	[1]
Al6061	Coconut shell	Graphene	67.5 to 89.5	178.28 to 246.23	NR	7.5 to 9.2	2.71 to 2.59	[25]
Al-Mg-Si	Maize stalk	None	6.80 to 20.20	50.86 to 85.60	43.42 to 70.25	7 to 14		[26]
Al6063	Palm kernel shell	None	335 to 615	102.45 to 190.14	10.25 to 14.00	7.5 to 13.75	NR	[21]
Al6063	Coconut shell	None	35.66 to 40.20	57.95 to 79.30	1.02 to 1.05 Mpa	NR	2.65 to 2.59	[27]
Al6063	Corn cob	None	27 to 59	247.65 to 52.35	NR	NR	2.66 to 2.44	[28]
Al-Mg-Si	Green plantain peel	Al_2O_3	87.60 to 101.04	93.94 to 175.29	6.50 to 15.63	3.5 to 12.1	NR	[22]
Al6061	Eggshell	None	32.32 to 37.13	NR	NR	NR	2.35 to 2.28	[29]
Al6061	Coconut shell	None	67.5 to 82.5	60 to 150	NR	NR	2.70 to2.57	[30]
Al6061	Sugarcane bagasse	None	66.75 to 71.25	152.45 to 198.75	NR	NR	NR	[31]
Al-Mg-Si	Eggshell	TiO_2	92 to 138	280 to 395	NR	NR	NR	[32]

Where NR means Not Reported

2. Materials and Methods

2.1 Materials

This study employed materials such as high-purity alumina, Al-Mg-Si (AA6063) alloy slabs, and cassava peels. The cassava peels were sourced from local cassava plantation farmers in Ede, located in the southwestern region of Nigeria.

2.2 Cassava peel processing

Heat treatment is widely recognized as an effective method for valorizing agro-waste residues, such as cassava peels, for engineering applications [33]. This process facilitates the production of inorganic ash, which is essential for elemental and compositional analyses. The cassava peels used in this study were initially sun-dried for several days to reduce moisture content and lower the cyanide levels. Sun-drying has been reported to reduce cyanide content by up to 90% without adversely affecting the nutritional or structural integrity of the peels [42]. Following sun-drying, the peels were oven-dried for 24 hours at 62 °C to eliminate residual moisture. Controlled oven-drying within the temperature interval of 46-100 °C has been found to minimize cyanide content further and enhance material stability [43]. The dried-out cassava peels were transferred into a metal chamber and subjected to open-air combustion. The resulting ash was then calcined in an electric muffle furnace for 185 minutes at 655 °C. This conditioning step yielded high-purity, thermally stable cassava peel ash (CPA), which is suitable for use as a reinforcing material in the fabrication of MMCs.

2.3 Composite synthesis and production

The two-stage stir casting methodology was adopted for synthesizing the Al-Mg-Si matrix composites incorporating particulates of cassava peel ash and alumina as reinforcement. This method is widely adopted in manufacturing agro-waste residue reinforced with MMCs due to its effectiveness in minimizing particulate agglomeration and guaranteeing uniform dispersion of reinforcement particulates throughout the matrix [44]. The process flowchart for the synthesis and production of the CPA/Alumina/Al-Mg-Si AMCs is illustrated in Fig. 1. The slabs of Al-Mg-Si alloy were liquefied within a graphite crucible placed inside a resistive furnace to obtain a molten state. The CPA and alumina powders were prepared and blended to achieve a combined reinforcement weight fraction of 10%, as detailed in Table 2. The particulates were thoroughly mixed and preheated at 250 °C prior to incorporation into the melt. Preheating has been shown to enhance the wettability and dispersion of agro-waste and ceramic reinforcements in metal matrices [19,44]. The preheated natural (CPA) and synthetic (alumina) reinforcements were gradually added to the molten Al-Mg-Si alloy at 750 °C and stirred consistently for 15 minutes. Magnesium was added at 0.001 wt.% to improve wettability. The mixture was then superheated to 880 °C to promote uniform distribution of the reinforcements and minimize clustering. A second round of stirring was carried out at this elevated temperature for another 15 minutes using a mechanical agitator. This completed the two-step stir casting process and enhanced the adhesion at the interface of the matrix-reinforcement particulates. The resulting molten composite was subsequently drenched into sand moulds prepared from kaolin, following the method described by [45] and allowed to cool under ambient conditions. The solidified CPA/Alumina/Al-Mg-Si composite ingots were removed, machined, and cut into standard test specimens. Each specimen was labeled correctly for identification and subjected to mechanistic property evaluation.

Table 2. Weight percent of CPA and alumina reinforcements.

S/N	Sample-ID	CPA (wt.%)	Alumina (wt.%)
1	CPA-0	0	10
2	CPA-2	2	8
3	CPA-4	4	6
4	CPA-5	5	5
5	CPA-6	6	4
6	CPA-8	8	2
7	CPA-10	10	0

Fig. 1. *Process flowchart for synthesizing CPA/alumina-reinforced Al-Mg-Si composites.*

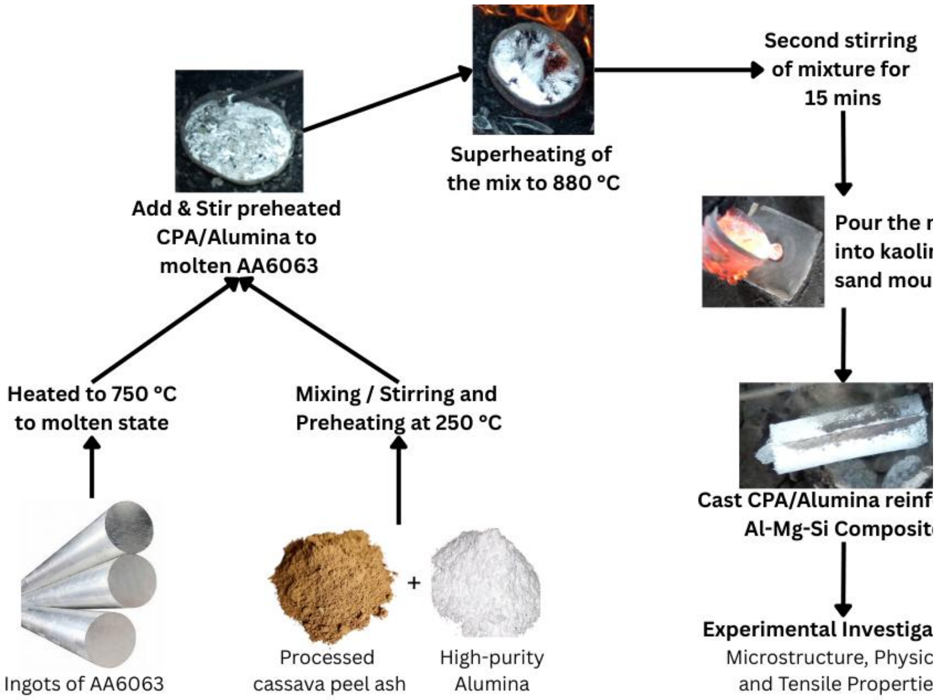

2.4 Microstructural investigation

Microstructural analyses were conducted on the as-prepared cassava peel ash particulates and the fabricated monolithic and hybrid CPA/Alumina/Al-Mg-Si AMCs. A FE-SEM (JSM-799F JEOL) fitted with an EDX spectrometer was employed to observe the morphology, particle dispersion, and interfacial bonding of the reinforcements within the matrix. In addition, elemental phase analysis and oxide composition were conducted with the aid of an XRD diffractometer and XRF spectrometer, providing insights into the chemical properties, crystallinity, and phase constituents.

2.5 Physical property measurement

The density of the reinforcement particles was measured using a pycnometer. For the fabricated CPA/Alumina/Al-Mg-Si AMCs, density and void content measurements were conducted in compliance with the ASTM D2734 guideline [46]. The theoretical density (ρ_{td}), experimental density (ρ_{ed}), and void fraction (V_d) was estimated using Equations 1, 2, and 3, respectively. To obtain the experimental density, each composite sample was first weighed using a high-precision digital analytical balance to determine its mass (M). The sample volume (V) was then calculated, adopting the buoyancy principle using the displacement method, in line with Archimedes' flotation technique [47].

$$\rho_{td} = Wt._{Al-Mg-Si} \times \rho_{Alumina} + Wt._{CPA} \times \rho_{CPA} + Wt._{Alumina} \times \rho_{Alumina} \quad (1)$$

$$\rho_{ed} = {}^{M}/_{V} \quad (2)$$

$$V_d = \frac{\rho_{td} - \rho_{ed}}{\rho_{td}} \times 100\% \quad (3)$$

2.6 Hardness performance

Hardness test was conducted on the fabricated CPA/Alumina/Al-Mg-Si composites with the aid of a hardness testing machine (Innovatest Falcon-500), in compliance with the ASTM E10 guideline [48]. A 10 mm diameter (D) steel ball indenter was used to apply a load (F) of 980.67 N across the surface of each composite sample, at a holding time of 10 seconds. The diameter of the resulting indentation (d) was estimated perpendicularly with the aid of a ×20 optical microscope integrated into the testing machine. The Brinell Hardness Number (BHN) was computed by employing Equation 4. For accuracy and consistency, three indentation measurements were recorded for each sample, with the average reading recorded as the Brinell hardness for the corresponding CPA/Alumina/Al-Mg-Si composite.

$$BHN = \frac{2 \times F}{\pi D(D - \sqrt{D^2 - d^2})} \tag{4}$$

2.7 Tensile properties test

The recommended tensile property tests for aluminum matrix composites include Young's modulus, percentage elongation, ultimate tensile strength (UTS), yield strength, toughness, and strain at failure [49,50]. The UTS test determines the maximum stress AMCs can endure before failure, while yield strength shows the stress level at which plastic deformation begins, a crucial parameter for AMCs subjected to constant or fluctuating loads. Ductility and toughness of AMCs are assessed through the percentage elongation at break, providing insight into the AMCs' ability to undergo deformation before fracture. The stiffness of the AMCs under load in structural components is measured by the Young's or elastic modulus, while strain at failure determines the brittleness or toughness of the fabricated AMCs relevant for applications where impact resistance is critical.

An Instron 1192 universal tensile testing instrument was employed in determining the tensile properties of the fabricated CPA/Alumina/Al-Mg-Si AMCs in compliance with the ASTM E8 guidelines [51]. The composite specimens for tensile testing were prepared to dimensions of 40 mm gauge length and 5 mm diameter, with testing conducted at a 1.0 mm/min crosshead speed in compliance with the recommended strain rate for aluminum-based composites. For each reinforced CPA/Alumina/Al-Mg-Si AMCs, the test was conducted in triplicate, and the resulting tensile stress-strain curves were analyzed to determine the yield strength, UTS, toughness, elongation at break, Young's modulus, and tensile strain at failure.

3. Results and Discussion

3.1 Characterization of reinforcement particulates

Fig. 2 presents the as-prepared cassava peel ash particulates (Fig. 2a) along with their corresponding microstructural features (Fig. 2b) and elemental composition obtained from EDX analysis (Fig. 2c). The findings of the chemical composition analysis, phase constituents, and physical properties of the reinforcement are equally presented and discussed, establishing their suitability as reinforcement materials.

3.1.1 Morphology, element, chemical, and phase characterization

The SEM micrograph of CPA presented in Fig. 2b shows a heterogeneous morphology having irregular, agglomerated submicron particles, which is typical of materials formed through thermal degradation of organic matter [33]. The particles exhibit non-uniform, roundish shapes with occasional longitudinal features, supporting their potential use in porous composites where increased interfacial surface area enhances matrix–particle bonding. No significant surface defects or sharp contours were observed, further indicating the material's suitability for uniform dispersion in metal matrix systems. This observation is consistent with the SEM results from [1,52,53].

The EDX elemental map result shown in Fig. 2c reveal a significant presence of oxygen (46.2 wt.%), silicon (21.0 wt.%), potassium (10.8 wt.%), aluminium (9.0 wt.%), calcium (5.3 wt.%), iron (4.8 wt.%), magnesium (1.2 wt.%), and phosphorus (0.4 wt.%). This observation indicates that the CPA is primarily composed of silica (SiO_2), followed by potassium oxide (K_2O) and aluminium oxide (Al_2O_3). The XRF analysis in Fig 3a confirms this elemental distribution, with a high silica content of 43.59%, consistent with values reported in previous studies [1,36,54,55]. Other oxide compositions recorded include Al_2O_3 (15.69%), K_2O (12.56%), CaO (11.73%), and Fe_2O_3 (8.46%). The XRD phase composition analysis shown in Fig. 3b confirms the presence of prominent silicate (SiO_2) phases and highlights the predominantly amorphous nature of CPA. The amorphous characteristics of CPA have also been reported by [56,57]. Additional phase peaks identified in this study include monoclinic calcium silicate (Ca_3SiO_5) and hexagonal ferric oxide (Fe_2O_3).

These findings suggest the likelihood of CPA to improve the hardness, thermal stability, and wear resistance when used as reinforcements in AMCs due to the high silica content (Figs. 3 and 4), which are key properties required for load-bearing and high-temperature environments [58]. In addition, the presence of K_2O and Al_2O_3 will significantly contribute to improved stiffness and rigidity of the composite matrix [44]. The CaO and Fe_2O_3 content will likely improve the mechanical strength and load-bearing potential of the CPA particulates, with CaO in particular aiding in porosity reduction due to its fluxing characteristics [59], improving particle-matrix adhesion and overall densification [60].

3.1.2 Particulate density characterization

The as-processed cassava peel ash and alumina exhibited density values of 2.68 g cm^{-3} and 3.98 g cm^{-3}, respectively. The CPA density aligns with previous findings [1], although it is slightly lower than the 2.95 g cm^{-3} reported by [61], yet falls within the general range of 2.5 – 3.0 g cm^{-3} for CPA [33]. The measured alumina density is also consistent with established literature values, deviating by only 0.19% [10]. The 32.66% density difference between CPA and alumina suggests that increasing the proportion of CPA in the composite formulation could contribute to overall weight reduction, which is an important advantage for lightweight structural applications such as automotive and aerospace. Conversely, increasing the alumina content would enhance the ceramic nature of the composite, likely improving hardness and stiffness.

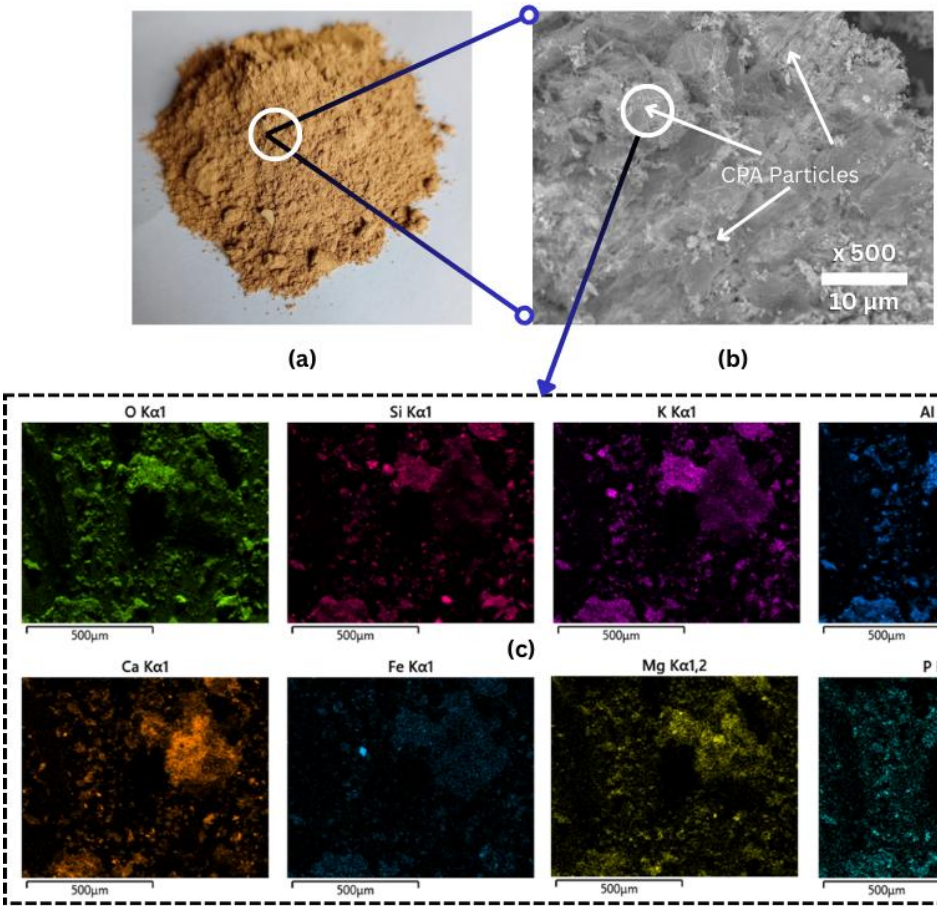

Fig. 2. *Physio-structural characterization of CPA particulates: (a) macroscopic view, (b) SEM micrograph, and (c) EDX mapping..*

Fig. 3. *(a) Chemical composition and (b) Elemental phase peaks of CPA particulates.*

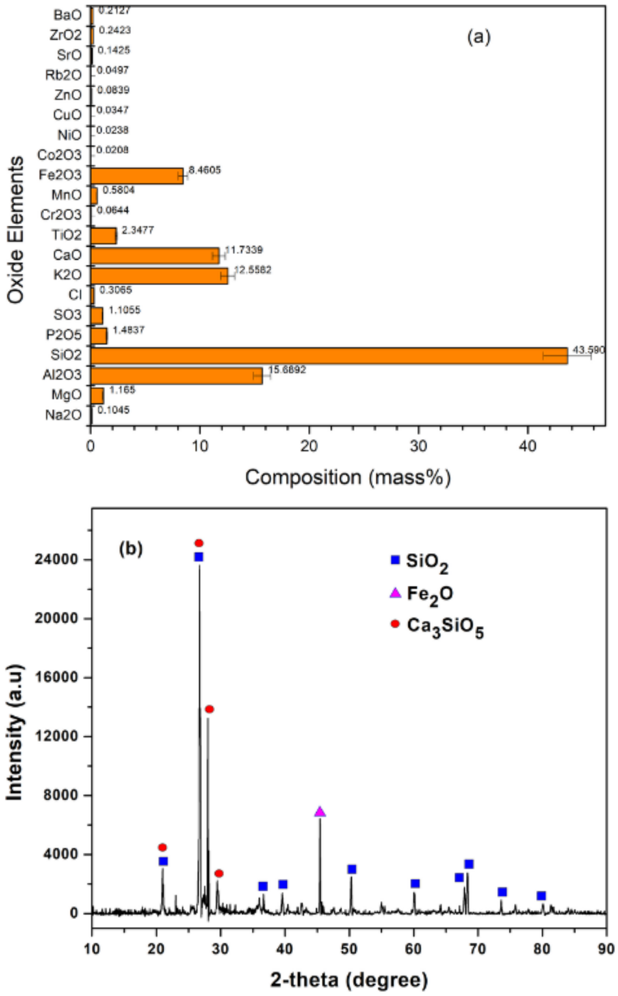

3.2 *Physio-structural and mechanical performance of the monolithic and hybrid composites*

3.2.1 *Microstructural characterization*

The SEM micrographs of the as-produced CPA/Alumina/Al-Mg-Si AMCs are presented in Fig. 4 for the fabricated monolithic and hybrid composites. The surface morphology of the monolithic CPA-0 composite with 10 wt.% alumina (Fig. 4a) appears uniform with well-dispersed alumina particulates within the Al-Mg-Si alloy matrix and no visible clustering. Sharp grain boundaries, minimal voids, and clean interfaces indicate good wettability and strong particle–matrix interaction. The monolithic CPA-10 composite with 10 wt.% CPA (Fig. 4b) as the only reinforcement, showed a heterogeneous morphology with irregular and agglomerated particulates dispersed within the Al-Mg-Si matrix. The rough surface texture and indistinct grain boundaries reflect the CPA particles' porous and non-uniform nature. These findings indicate that while the microstructure of CPA-0 supports strong interfacial bonding, low porosity, and efficient load transfer, enhancing the composite's stiffness and strength due to alumina's high density, the irregular and agglomerated nature of CPA-10 may hinder load transfer. Strong interfacial bonding, desirable for structural applications, is essential for efficient load transfer during mechanical loading [62]. However, the porous and non-uniform features of CPA could enhance energy absorption and interfacial anchoring in structural applications [63].

The SEM microstructure of the hybrid CPA-2 (8 wt.% alumina and 2 wt.% CPA) is shown in Fig. 4(c). A relatively dense surface morphology was observed with elongated particulates and no signs of severe agglomeration. Compared to CPA-10, the improved dispersion is attributed to the higher alumina content, while compared to CPA-0, the introduction of CPA results in the appearance of some voids, reflecting the influence of its porous nature. The moderate heterogeneity and visible reinforcement–matrix interfaces suggest a good balance, promoting effective dispersion and interfacial bonding, likely contributing to improved mechanical properties. Fig.

Fig. 4. *SEM micrograph of the fabricated monolithic and hybrid CPA/Alumina/Al-Mg-Si AMCs.*

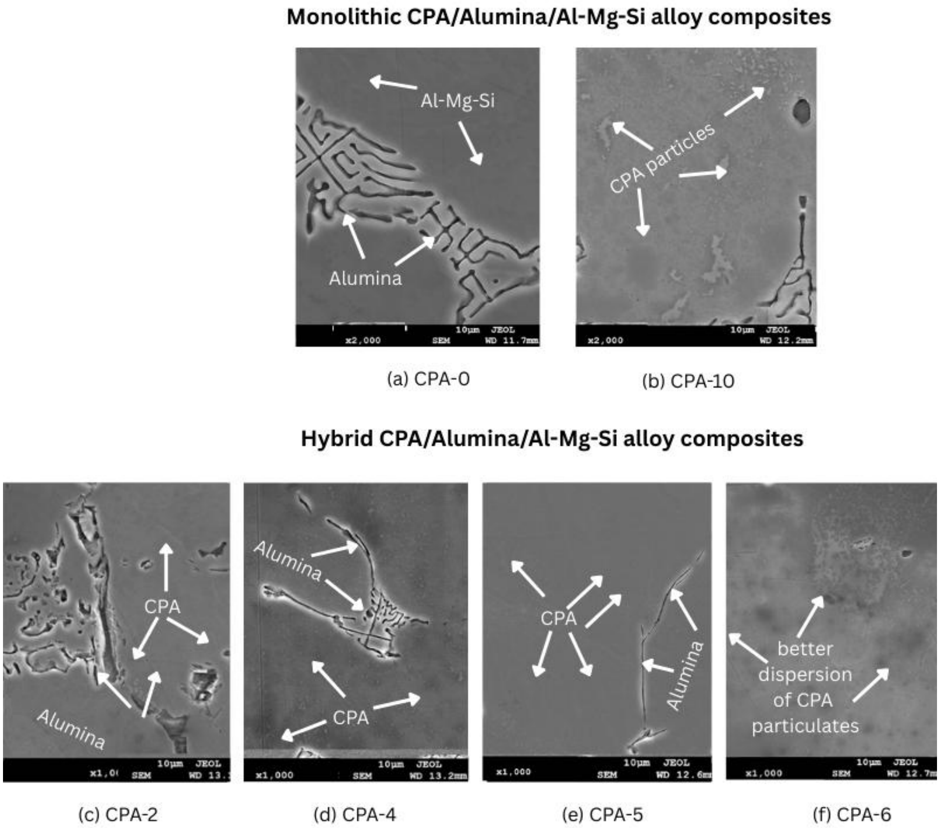

4(d) shows the microstructure of hybrid CPA-4 with alumina decreasing to 6 wt.% and CPA increasing to 4 wt.% compared to CPA-0. Compared to CPA-2, the slight reduction in alumina and increase in CPA introduce more surface irregularities and interfacial complexity, resulting in a moderately dense and well-integrated matrix with elongated particulates and distinct matrix–particle interfaces. This decrease in synthetic reinforcements may reduce composite stiffness and strength, while the increase in CPA reinforcements may benefit toughness, and energy absorption due to the porous morphology of cassava peel ash (Fig. 2).

Fig. 4(e) presents the SEM image of hybrid CPA-5, with equal amounts of alumina (5 wt.%) and CPA (5 wt.%). The surface shows moderately uniform dispersion with elongated particulates and better structural integration compared to CPA-10 but slightly less refined than CPA-2 and CPA-0. The balanced reinforcement phase introduces visible surface irregularities, while the observed interfacial adhesion and moderate voids suggest a compromise between strength and toughness in the CPA-5 composite. CPA-6 composite with 4 wt.% alumina and 6 wt.% CPA exhibits a moderately heterogeneous microstructure with dispersed particulates, interfacial voids, and surface irregularities as presented in Fig. 4(f), compared to CPA-4 and CPA-5. The increased CPA content enhanced porosity and surface irregularity, while the reduced alumina decreased structural compactness, suggesting a trade-off between rigidity and ductility. The microstructure of the 2 wt.% alumina and 8 wt.% CPA (CPA-8) presented in Fig. 4(g) shows an irregular particle dispersion, high porosity with increased voids, and uneven particle bonding. Irregular boundaries and heterogeneity are more pronounced compared to CPA-6, suggesting that interfacial gaps may reduce tensile strength and stiffness while enhancing thermal shock resistance and energy absorption [64,65].

Generally, increasing the CPA content while reducing alumina leads to a distinct microstructural transition from a compact, load-bearing architecture to a more porous, energy-absorbing structure. These observations align with previous findings on the influence of CPA on the microstructure of aluminium matrix composites [1,24]. Hybrid compositions such as CPA-4 and CPA-5 appear to strike an optimal balance between mechanical strength and flexibility, whereas the monolithic extremes CPA-0 and CPA-10 tend to emphasize either stiffness or toughness, respectively. The observed interfacial compatibility and wettability between the reinforcements and the matrix attest to the effectiveness of the two-stage stir casting technique employed in this study.

Table 3. *Density and estimated void percent of CPA/Alumina/Al-Mg-Si composites.*

S/N	Sample-ID	Theoretical density (g cm^{-3})	Experimental density (g cm^{-3})	Void (%)
1	CPA-0	2.780	2.735	1.620
2	CPA-2	2.761	2.722	1.424
3	CPA-4	2.743	2.701	1.526
4	CPA-5	2.734	2.698	1.311
5	CPA-6	2.725	2.692	1.212
6	CPA-8	2.707	2.682	0.925
7	CPA-10	2.689	2.637	1.944

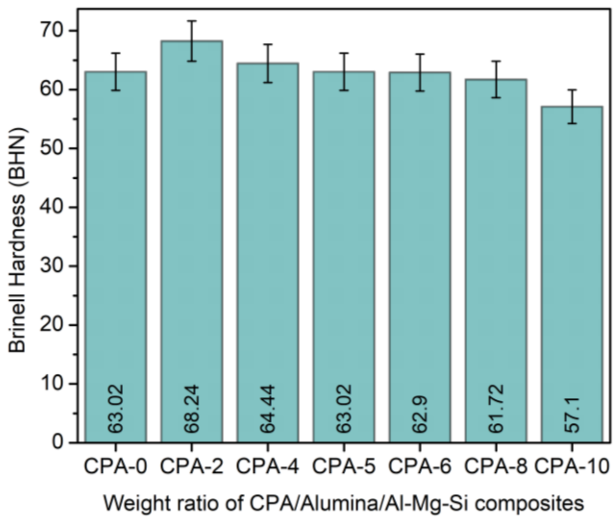

Fig. 5. *Hardness results of CPA/Alumina reinforced Al-Mg-Si AMCs.*

3.2.2 Density and void analysis

Table 3 presents the theoretical and experimental densities and the estimated percent void content for the monolithic and hybrid CPA/Alumina/Al-Mg-Si composite. These measurements were used to assess the compactness and structural integrity of the composites by comparing theoretical and experimental densities and evaluating the void content. The theoretical and experimental densities are observed to decrease progressively with an increase in CPA content and a decrease in alumina, consistent with the individual particulate densities reported earlier for CPA (2.68 g cm^{-3}) and alumina (3.98 g cm^{-3}). This indicates that incorporating CPA as a partial or full replacement for alumina in AMCs enables the development of lightweight materials, making them particularly suitable for structural applications where lightweight design is critical. Such applications include the automobile industry, where reduced weight contributes to lower fuel consumption [66]; the aerospace sector, where it enhances speed and efficiency; and in construction and interior design, where lightweight materials ease handling and installation [6].

CPA-0 and CPA-10 recorded the highest (2.780 g cm^{-3} and 2.735 g cm^{-3}) and lowest (2.689 g cm^{-3} and 2.637 g cm^{-3}) theoretical and experimental densities by the monolithic composites of CPA-0 and CPA-10, respectively. Among the hybrid composites, CPA-2 with the lowest CPA had the highest theoretical and experimental densities of 2.761 g cm^{-3} and 2.722 g cm^{-3}, respectively, while CPA-8 with the lowest alumina recorded the lowest theoretical and experimental densities of 2.707 g cm^{-3} and 2.682 g cm^{-3}, respectively. These findings align with previous research where agro-waste residues are increasingly favored as reinforcements in MMCs due to their ability to effectively reduce composite weight while maintaining or enhancing mechanical performance [67,68].

The void fraction accounts for the discrepancies between the theoretical and experimental densities of the fabricated composites, with values ranging from 0.925% (CPA-8) to 1.944% (CPA-10). The reduced void percentage exhibited by CPA-8 indicates a favorable reinforcement packing structure and good wettability at this composition, while the particulate agglomeration due to the porous morphology of CPA may have accounted for the high void content in CPA-10. Although the void content in all samples remains below the 4% threshold typically recommended for AMCs, ASTM D2734 indicates that void fractions can significantly affect a composite's

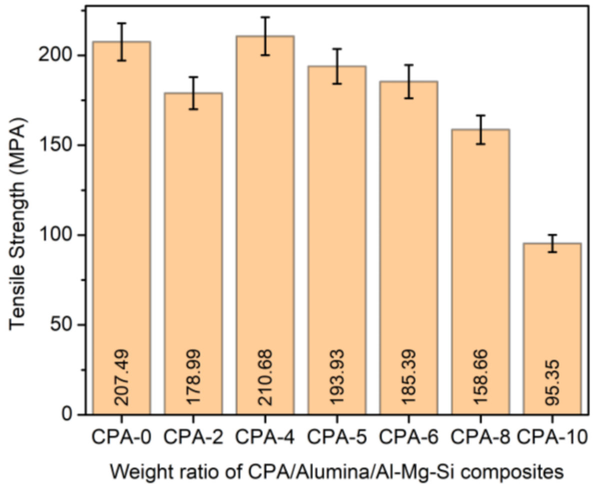

Fig. 6. *Variation in tensile strength results for the fabricated CPA/Alumina/Al-Mg-Si AMCs.*

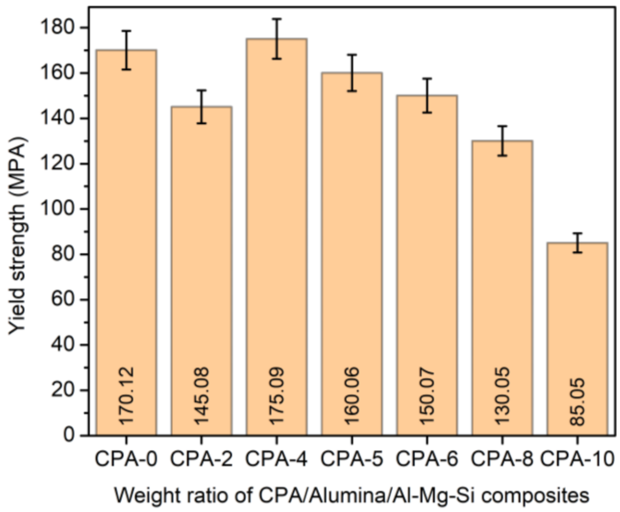

Fig. 7. *Variation in yield strength results for the fabricated CPA/Alumina/Al-Mg-Si AMCs.*

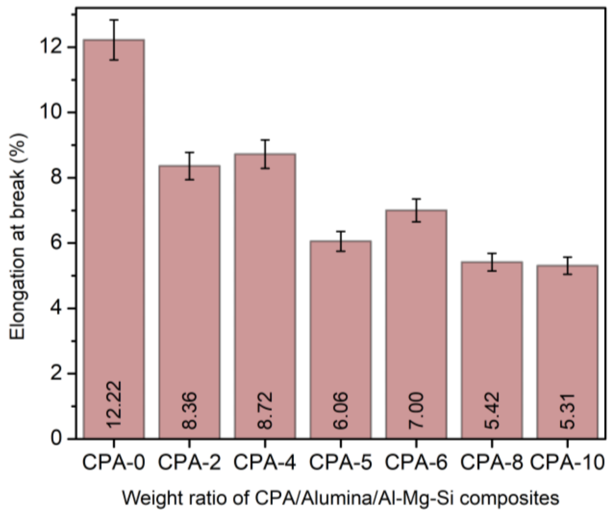

Fig. 8. *Variation in ductility results for the fabricated CPA/Alumina/Al-Mg-Si AMCs.*

mechanical performance, with higher values resulting in lower fatigue resistance [46]. The relatively high void content of 1.620% observed in CPA-0 can be linked to the brittle nature of alumina and weaker wetting within the molten matrix (Fig. 4a). The hybrid composition of CPA-5 and CPA-6 appears to achieve an optimal balance between densification and particle dispersion, as reflected by their relatively low void content values of 1.311% and 1.212%, respectively. These findings reinforce earlier microstructural observations (Fig. 4) and suggest that combining CPA and alumina in moderate proportions improves matrix reinforcement interaction and minimizes porosity.

3.2.3 Hardness performance

Fig. 5 presents the hardness result of the monolithic and hybrid CPA/Alumina/Al-Mg-Si AMCs, with values ranging from 57.10 BHN (CPA-10) to 68.24 BHN (CPA-2). These results align with the previously discussed microstructural features, the particulates' reinforcement compositions, density, and void trends. Fig. 5 reveals that CPA-2 exhibited the highest hardness, followed by CPA-4 (64.44 BHN), surpassing CPA-0, which contains a higher proportion of harder and denser ceramic reinforcement, alumina. The synergistic effect and interfacial strengthening mechanisms of the composite reinforcement account for this observation. Although CPA-0 consists of 10 wt.% alumina, a dense and hard ceramic (3.98 g cm^{-3}), its microstructure (Fig. 4a) shows compactness but limited interfacial reactivity. This is because alumina often suffers from poor wettability in aluminum matrices [69,70]. Thus, the addition of a small amount of CPA (2 wt.%) in CPA-2 enhanced interfacial bonding due to the porous and reactive surface of CPA particulates, which contain oxide constituents such as SiO_2, Al_2O_3, Fe_2O_3, and CaO (Fig. 2a). These oxides are known to enhance surface hardness and provide microstructural rigidity when well-dispersed, promoting localized diffusion and better matrix anchoring, especially under stir casting conditions [71,72]. Furthermore, the microstructural interaction between alumina and CPA in CPA-2 likely enhanced surface resistance to indentation, explaining its superior hardness.

Hardness remains relatively high at lower CPA levels (CPA-0 to CPA-4) due to the balanced presence of alumina (significant for its load-bearing capacity), the minimal porosity, compact microstructure, strong reinforcement-matrix bonding, and moderate void content (1.424% for CPA-2 and 1.526% for CPA-4), suggesting that adequate reinforcement packing and wettability were achieved, minimizing microcrack propagation and local stress concentrations under indentation. Conversely, a further increase in CPA levels (CPA-5 to CPA-10), a steady reduction in hardness is observed, with CPA-10 reporting the lowest value. This decline can be attributed to increased porosity in CPA's morphology (Fig. 4) at higher values, with the gradual reduction in alumina resulting in a softer and less structurally rigid composite matrix. Despite the presence of hard oxides (Fe_2O_3, Al_2O_3, and SiO_2) in CPA, the weaker interfacial bonding at higher CPA ratios compromised the load-transfer efficiency due to a reduction in matrix continuity. This is particularly evident in CPA-10, which exhibited both the highest void content (1.944%) and highly disrupted microstructure (Fig. 4g), correlating with the lowest measured hardness (57.10 BHN).

This finding is consistent with the observation by [24], which reported a decrease in hardness with increasing CPA content, even when hybridized with silicon carbide (SiC) in Al-Mg-Si alloy composites. Similarly, a CPA-induced hardness of 83.45 BHN, lower than values obtained with coconut shell ash (88.67 BHN) and rice husk ash (93.55), was reported at 15 wt.% for each of the agro-waste residues reinforced with AA6063 [17]. Despite its lower intrinsic hardness, CPA still demonstrated a substantial strengthening effect in the present study. For instance, CPA-10 achieved a hardness of 57.10 BHN, representing a 128.4% increase compared to the baseline AA6063 alloy (25 BHN), thereby confirming CPA's potential to enhance surface hardness. This suggests that, as an agro-waste-derived reinforcement, CPA can be effectively used to develop lightweight composites with relatively high hardness, broadening their applicability in structural and wear-resistant components.

3.2.4 Tensile strength performance

For tensile strength performance, measured values ranged from 95.39 MPa for the monolithic CPA-10 to 210.68 MPA for the hybrid CPA-4, exhibiting a distinct non-linear trend observed across the reinforcement ratios (Fig. 6). The CPA-4 sample, comprising 6 wt.% alumina and 4 wt.% CPA, recorded the highest ultimate tensile strength (UTS) value, surpassing even the monolithic alumina-reinforced CPA-0, which had a UTS of 207.49 MPa. This remarkable performance suggests that the combined contribution of alumina's stiffness and CPA's oxide-rich composition (Fig. 3a), coupled with its anchoring morphology (Fig. 4d), significantly enhanced load transfer and matrix interaction. Additionally, CPA-4 exhibited a void content of 1.526% (Table 3), which is ideal for maintaining load path integrity. A similar non-linear trend has been reported for cassava peel ash reinforced Al-Mg-Si alloy by [24]. Notably, CPA-2 exhibited a dip in UTS (178.99 MPa) despite still containing 8 wt.% alumina. This drop is likely due to a minor disruption in particle packing and matrix continuity introduced by the initial 2 wt.% CPA addition, as confirmed by the microstructural analysis (Fig. 4c), which revealed moderate voids and less uniform particle distribution. Furthermore, the sharp rise in UTS from CPA-2 to CPA-4 reflects the stabilization of particle dispersion and improved interfacial bonding when CPA is incorporated at a more synergistic proportion, resulting in enhanced load distribution and crack-bridging. Similar observations have been reported in the literature for hybrid composites reinforced with small amounts of bio-based ceramics (like fly ash or RHA), where improved mechanical strength is achieved through better bonding and stress dissipation than in single-reinforcement [40,61,73,74].

Beyond CPA-4, a progressive reduction in UTS is observed as the alumina content decreases and the CPA content increases (CPA-5 to CPA-10). This reduction correlates with the decline in ceramic rigidity, increase in porosity (Table 3), and worsening particle agglomeration (Figs. 4b and 4e-g), all of which degrade matrix integrity and diminish the composite's ability to withstand tensile loading. These observations are consistent with the earlier trends reported for density (Table 3) and hardness (Fig. 5). The sharp drop in the tensile strength observed in CPA-10 can be attributed to CPA's highly irregular and porous morphology, poor dispersion, and weak bonding characteristics, while the superior performance of CPA-0 is linked to alumina's high density and inherent ceramic hardness. The tensile strength obtained in this study for monolithic CPA-10 (10 wt.% CPA) is 175%, 170%, and 153% higher than the values reported for 15 wt.% CPA, 15 wt.% CSA, and 15 wt.% RHA, respectively, by [17], but remains approximately 50% lesser than the value reported for 100 wt.% CPA reinforced Al-Mg-Si alloy by [24].

3.2.5 Yield strength performance

The yield strength shows the stress level at which a composite material deforms plastically. In this study, the yield strength for the fabricated CPA/Alumina/Al-Mg-Si AMCs shown in Fig. 7 varied from 85.05 MPa (monolithic CPA-10) to 175.09 MPa (hybrid CPA-4), with a trend pattern consistent with the tensile strength (Fig. 6a). The presence of high-hardness oxides such as SiO_2, Fe_2O_3, Al_2O_3, and CaO in CPA (Fig. 3a) contributes to the strengthening of the hybrid CPA-4 composite, while at higher CPA content and reduced alumina content (CPA-5 to CPA-10), yield strength experienced a steady decline correlating with the increased void fractions and reduced ceramic rigidity (Table 3). Furthermore, particle wetting and dispersion become less effective with increasing CPA content (Fig. 4), resulting in matrix discontinuities and reduced composites' resistance to permanent deformation under load. A similar observation was reported for a hybrid RHA/Alumina reinforced Al-Mg-Si alloy, with yield strength decreasing with increasing RHA content [75]. This suggests that yield strength depends not only on the presence of hard phases but also on the quality of interfacial distribution and stress distribution within the composite [76–78]. The hybrid CPA-4 composite showed uniform dispersion, with the reinforcements acting as barriers to dislocation motion, delaying the onset of yielding. However, the matrix fails prematurely under load for a porous, non-uniform, and irregularly shaped monolithic CPA-10 composite.

3.2.6 Elongation at break behavior

The elongation at break, a key indicator of ductility, reflects the amount of strain a composite material experiences before fracturing. Several interrelated factors, including void content, particulate dispersion, interface strength, and reinforcement morphology, influence ductility in MMCs. In this study, the percentage elongation at break for the fabricated CPA/Alumina/Al-Mg-Si composites (Fig. 8) was lowest in monolithic CPA-10 (5.31%) and highest in monolithic CPA-0 (12.22%). Despite alumina being a stiff ceramic, the high ductility observed in CPA-0 can be attributed to its well-dispersed morphology (Fig. 4a), uniform particle distribution, relatively low void content (1.620%), and strong interfacial bonding, which collectively enabled the matrix to deform plastically without premature crack propagation. This behavior contrasts with the hybrid CPA-reinforced composites, where ductility decreased as CPA content increased and alumina content decreased (CPA-2 to CPA-10). This reduction is attributed to CPA's porous and irregular morphology, which introduces microstructural discontinuities and stress concentrators, thereby promoting early failure under tension [56]. Although CPA-4 exhibited the highest tensile and yield strengths, its moderately low elongation (8.72%) highlights the classic strength–ductility trade-off observed in MMCs [79,80].

Notably, a slight increase in ductility was observed at CPA-6, with elongation rising to 7.00%, about 16% higher than CPA-5 (6.06%), before decreasing again in CPA-8. This localized improvement in CPA-6 is supported by void content and microstructural evidence, where CPA-6 recorded a slightly lower void content (1.212%) compared to CPA-5 (1.311%), suggesting improved particle–matrix cohesion, reduced crack initiation sites, and more uniform deformation under tensile load. The poor bonding and high CPA dominance in CPA-8 suggest why the temporary increase in elongation by CPA-6 was not sustained in CPA-8, despite the latter having the lowest void content of 0.925%. Similar non-monotonic trends in elongation with increasing agro-waste reinforcement have been reported in the literature. A reduction in ductility from 7.75% (6 wt.% RHA) to 5.37% (10 wt.% RHA) in Al6061–Cu–Mg composites was observed by [74]. An inconsistent elongation trend with increasing RHA content was reported by

[75]. A comparable pattern was observed where increasing green plantain peel ash (GPPA) and alumina in AA6063 composites led to a consistent decline in ductility [22].

3.2.7 Young's modulus performance

The Young's modulus describes a composite's resistance to elastic deformation under applied stress. Higher modulus values indicate stiffer materials, whereas lower values suggest increased flexibility. Fig. 9 presents the Young's modulus results for the fabricated CPA/Alumina/Al-Mg-Si AMCs, with values varying from 9.58 GPa for monolithic CPA-10 to 18.12 GPa for hybrid CPA-2. This variation highlights the influence of reinforcement composition on the stiffness of the composites. The high modulus observed in CPA-2 may be attributed to its elevated ceramic content and the presence of stiff oxides such as K_2O and Al_2O_3 in CPA, which enhance elastic load bearing without significant deformation. A strong and balanced elastic performance was also observed in CPA-0 (15.63 GPa), CPA-4 (15.81 GPa), and CPA-5 (15.34 GPa), suggesting effective ceramic dispersion and reinforcement-matrix interaction. These samples also correspond to relatively high tensile and yield strengths, indicating a partial alignment between stiffness and overall mechanical performance [15,81]. Like the trend observed in elongation at break, CPA-6 showed a notable deviation from the monotonic declining stiffness pattern, with a sharp increase to 17.80 GPa, followed by a drop to 12.35 GPa in CPA-8. This suggests that elastic stiffness may be retained or improved when matrix continuity is preserved, as supported by its relatively low void content (Table 3). However, the sharp decline in CPA-8 and CPA-10 confirms that excessive CPA content weakens elastic performance, likely due to its porous morphology, poor particle dispersion, and reduced structural cohesion. These observations are consistent with findings in GPPA/alumina-reinforced AA6063 composites [22] and bean pod ash (BPA) reinforced AA6063 AMCs [6], where excessive agro-waste reinforcement led to decreased stiffness and mechanical degradation.

3.2.8 Toughness behaviour

Fig. 10 shows the result of the toughness values obtained from the tensile tests for the fabricated CPA/alumina-reinforced Al-Mg-Si composites. A steady decline in toughness is observed with an increase in CPA content and a decrease in alumina content, with the exception of a slight rebound at CPA-6. This local increase aligns with trends seen in other tensile properties, such as Young's modulus (Fig. 9) and ductility (Fig. 8), and is attributed to lower void content and improved matrix continuity at that composition. Toughness ranged from 5.55 J in CPA-0 (monolithic alumina) to 0.81 J in CPA-10 (monolithic CPA), indicating a substantial reduction in the energy dissipation capability of the composites as CPA becomes the dominant phase. A combination of strength, ductility, reinforcement-matrix bonding, porosity, and particle morphology governs toughness in MMCs [82,83]. In this study, the reduced toughness at higher CPA content is linked to the porous and irregular morphology of CPA (Fig. 2), which introduces interfacial discontinuities and weakens particle–matrix adhesion. These structural deficiencies promote early fracture and lower energy dissipation [15]. The results are consistent with findings in the literature, where increasing agro-waste content, such as CSA, bamboo stem ash, and RHA, has similarly led to decreased toughness due to poor interfacial bonding and increased porosity [75,81]. A reduction in toughness has also been reported with decreasing proportions of hard ceramic reinforcements such as SiC, due to diminished stiffness and compromised load transfer capability [24,84,85].

3.2.9 Strain at failure behaviour

The strain at failure helps to determine the total deformation (plastic and elastic) that a composite material undergoes before fracture by measuring the composite's ability to endure elongation under tensile loading. Fig. 12 presents the strain at failure for each of the CPA/Alumina/Al-Mg-Si composites fabricated in this study, with values ranging from 0.0531 mm/mm (CPA-10) to 0.1222 mm/mm (CPA-0). A distinct reduction in strain capacity is observed with increasing CPA content and decreasing alumina content, with minor rebounds at CPA-4 (0.0872 mm/mm) and CPA-6 (0.0700 mm/mm). The deviations are attributed to the synergistic reinforcement effect between CPA and alumina in CPA-4, and the enhanced matrix bonding and reduced void content in CPA-6, which enhance structural continuity and deformation tolerance. CPA-10 recorded the lowest strain at failure (0.0531 mm/mm), which is consistent with its lowest UTS, yield strength, toughness, and elongation, and is further supported by its high void content (1.944%), severely disrupted matrix, and particle agglomeration (Fig. 4b). These structural deficiencies contribute to reduced crack resistance and promote early fractures. The findings

Fig. 9. *Variation in Young's modulus results for the fabricated CPA/Alumina/Al-Mg-Si AMCs.*

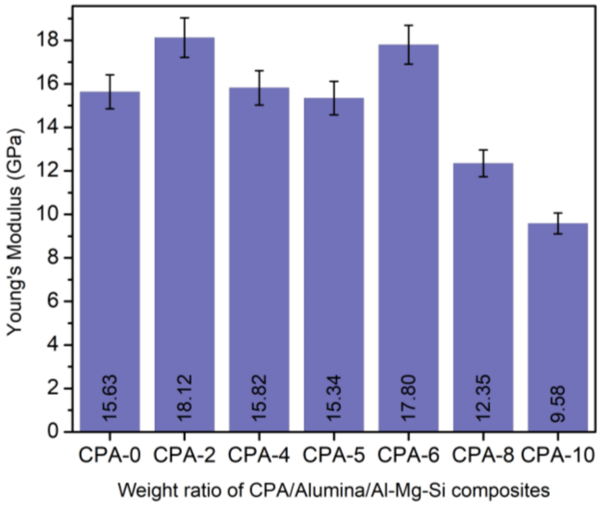

Fig. 10. *Variation in toughness results for the fabricated CPA/Alumina/Al-Mg-Si AMCs.*

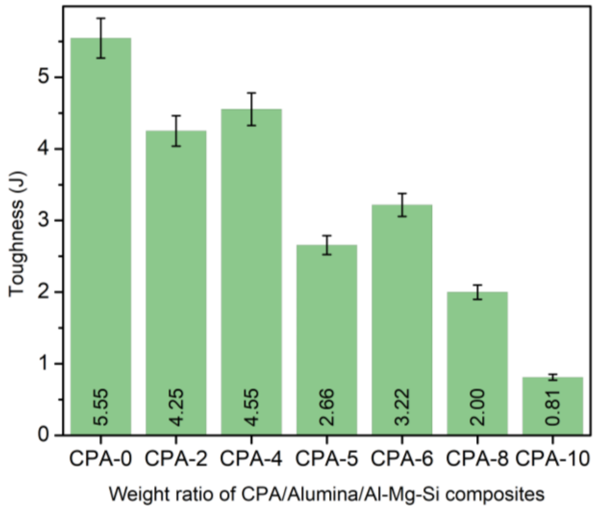

Fig. 10. *Variation in toughness results for the fabricated CPA/Alumina/Al-Mg-Si AMCs.*

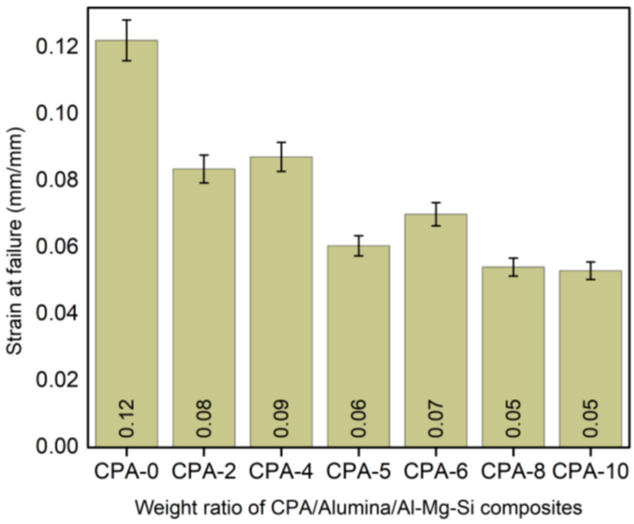

suggest that increasing CPA content elevates stress concentration and impairs interfacial cohesion, ultimately leading to premature failure under tensile stress [6,86]. This behavior is consistent with reports in the literature, where strain at failure decreased with increasing content of hard ceramic reinforcements such as SiC [87] and boron carbide (B_4C) [88], due to their inherent brittleness and limited ductility contribution to the matrix.

3.3 *Implications of mechanical performance and potential applications*

The comprehensive mechanistic performance of the variations of each CPA/Alumina/Al-Mg-Si composite fabricated in this study is presented in Table 4. The wear resistance of the different composites reported was obtained from the tribological results reported in a previous study [1]. These mechanical properties provide a strong foundation for assessing the optimal compositions for targeted engineering applications, determining the suitability of the composites for load-bearing, energy-absorbing, or wear-resistant functions.

The results show that CPA-4 demonstrated the highest tensile strength (210.68 MPa) and yield strength (175.09 MPa), with good hardness (64.44 BHN) and moderate toughness and ductility, making it the most balanced composite for structural applications. CPA-0, composed solely of alumina reinforcement, exhibited the highest toughness (5.55 J), ductility (12.22%), and strain at failure (0.1222 mm/mm), indicating its superior capacity for energy absorption and plastic deformation. CPA-2 recorded the highest hardness (68.24 BHN) and Young's modulus (18.12 GPa), suggesting its suitability in applications requiring high stiffness and surface wear resistance.

CPA-6 showed a minor rebound in multiple properties such as strain at failure (0.0700 mm/mm), toughness (3.22 J), and Young's modulus (17.80 GPa), supported by its low porosity (1.212%). This indicates a transitional reinforcement phase where elastic behavior and deformation tolerance are partially retained due to improved particle–matrix interaction. On the other hand, CPA-10, with the highest CPA content, recorded the lowest values across most mechanical properties, tensile strength (95.35 MPa), yield strength (85.05 MPa), toughness (0.81 J), and strain at failure (0.0531 mm/mm), but demonstrated the highest wear resistance (1.280 mm/mm^3), making it suitable for non-load-bearing, wear-intensive applications.

The mechanical property rankings of the CPA/Alumina-reinforced Al-Mg-Si alloy compiled in Table 4 can be correlated to suggest areas of application. For instance, CPA-0 is recommended for components requiring superior ductility and energy absorption, such as automotive panels, crumple zones, crash bars, or structural braces. CPA-2 and CPA-6 are ideal for moderate-load structural applications where stiffness and surface hardness are prioritized, such as gear casings, bushings, covers, and moderate frame connectors. CPA-4 stands out as the best choice for high-strength lightweight structures, including aerospace interior frames, vehicle chassis parts, and load-bearing joints. CPA-5 is recommended for moderate-load applications requiring strength and flexibility, such as tool handles and panels. CPA-8 and CPA-10, due to their excellent wear resistance but low strength and ductility, are recommended for applications such as flooring tiles, wall protection panels, internal wear plates, lining sheets, low-load brake pads, and non-structural sliding components.

4. Conclusion

The present study assessed the microstructural and mechanistic performance of Al-Mg-Si alloy reinforced with cassava peel ash and alumina particulates mixed in varying proportions to produce monolithic and hybrid composites. The findings show that:

- Cassava peel ash exhibits a heterogeneous distribution, irregular morphology, high porosity, and a high silica content, as confirmed by XRF and XRD analyses.
- The density and porosity of the fabricated composites slightly increased with increasing CPA content, influencing structural compactness.
- CPA-2 recorded the highest hardness performance of 68.24 BHN due to the stiff oxide-rich CPA contribution.
- Tensile strength and yield strength were highest in CPA-4, indicating good synergistic performance between the alumina and CPA particulates.
- Ductility declined with increased CPA content, as CPA-0 with monolithic alumina reinforcement recorded the highest percentage elongation potential.
- The highest stiffness was observed in CPA-2, while CPA-6 recorded a minor rebound in its Young's modulus performance due to better matrix continuity and reduced void content.
- Toughness decreased with increased CPA content, with CPA-0 absorbing the most energy before fracture.
- The total deformation capacity declined steadily with increased CPA content from CPA-0 to CPA-10.

These findings demonstrate the viability of cassava peel ash as a sustainable, eco-friendly, and lightweight engineering material capable of improving the structural and mechanistic performance of aluminum alloys such as AA6063, thereby broadening their range of engineering and structural applications. Notably, enhanced performance was achieved when cassava peel ash was optimally integrated with traditional ceramic reinforcements like alumina.

Table 4. *Detailed summary of the mechanical performance of CPA/Alumina/Al-Mg-Si composites.*

Property-ID	**CPA-0**	**CPA-2**	**CPA-4**	**CPA-5**	**CPA-6**	**CPA-8**	**CPA-10**	**Ref.**
Density (g cm^3)	2.74	2.72	2.70	2.70	2.69	2.68	2.64	This study
Porosity (%)	1.62	1.42	1.53	1.31	1.21	0.92	1.94	This study
Hardness (BHN)	63.02	68.24	64.44	63.02	62.90	61.72	57.10	This study
Tensile strength (MPa)	207.49	178.99	210.68	193.93	185.39	158.66	95.35	This study
Yield strength (MPa)	170.12	145.08	175.09	160.06	150.07	130.05	85.05	This study
Elongation at break (%)	12.22	8.36	8.72	6.06	7.00	5.42	5.31	This study
Young's modulus (GPa)	15.63	18.12	15.82	15.34	17.80	12.35	9.58	This study
Toughness (J)	5.55	4.25	4.55	2.66	3.22	2.00	0.81	This study
Strain at failure (mm/mm)	0.12	0.08	0.09	0.06	0.07	0.05	0.05	This study
Wear resistance (mm/mm^3)	0.455789	0.627353	0.628931	0.682594	0.917431	1.261034	1.28041	[1]

Declarations

Data availability Data will be made available upon reasonable request.

Funding This study received no funding.

Competing interests Authors declare no known competing or financial interests.

References

[1] F. Ben, P.A. Olubambi, In-situ reinforcement of AA6063/Al2O3 hybrid composite: comparative wear and hardness evaluation of Manihot esculenta and green Plantago major particulates, Discov. Appl. Sci. 6 (2024) 1–19. https://doi.org/10.1007/s42452-024-05946-7.

[2] M.B. Karamis, A. Tasdemirci, F. Nair, Failure and tribological behaviour of the AA5083 and AA6063 composites reinforced by SiC particles under ballistic impact, Compos. Part A 34 34 (2003) 217–226. https://doi.org/10.1016/S1359-835X(03)00024-1.

[3] M.A. Wahid, A.N. Siddiquee, Z.A. Khan, Aluminum alloys in marine construction: characteristics, application, and problems from a fabrication viewpoint, Mar. Syst. Ocean Technol. 15 (2020) 70–80. https://doi.org/10.1007/s40868-019-00069-w.

[4] K.K. Pius, N.O. Ongwen, M. Mageto, V. Odari, F.M. Gaitho, DFT-Based Study, (2023) 213–226.

[5] P.P. Seth, O. Parkash, D. Kumar, Structure and mechanical behavior of in situ developed Mg2Si phase in magnesium and aluminum alloys – a review, RSC Adv. 10 (2020) 37327–37345. https://doi.org/10.1039/D0RA02744H.

[6] F. Ben, P.A. Olubambi, Investigating the mechanical performance of innovative bean pod ash particulates reinforced in AA6063 alloy for construction and building applications, MRS Adv. (2025). https://doi.org/10.1557/s43580-025-01168-0.

[7] J. Gong, G.B. Olson, D.R. Snyder, Al—Mg—Si alloys for applications such as additive manufacturing, 20200385845, 2023. https://patents.justia.com/patent/11773468.

[8] A. Devaraju, A. Kumar, B. Kotiveerachari, Influence of addition of Grp/Al2O3p with SiCp on wear properties of aluminum alloy 6061-T6 hybrid composites via friction stir processing, Trans. Nonferrous Met. Soc. China 23 (2013) 1275–1280. https://doi.org/10.1016/S1003-6326(13)62593-5.

[9] A.A. Adediran, K.K. Alaneme, I.O. Oladele, E.T. Akinlabi, Microstructural characteristics and mechanical behaviour of aluminium matrix composites reinforced with Si-based refractory compounds derived from rice husk, Cogent Eng. 8 (2021) 1–17. https://doi.org/10.1080/23311916.2021.1897928.

[10] F. Ben, P.A. Olubambi, Investigating the Tribological Behavior of Bioinspired Surfaces in Agro-waste and Alumina Reinforced AA6063 Matrix Composites, Vacuum 230 (2024) 1–17. https://doi.org/10.1016/j.vacuum.2024.113687.

[11] O.A. Ogunsanya, A. Adewale Akinwande, R. Raj Mohan, H. Talabi, M. Saravana Kumar, M. Vignesh, A. Bhowmik, Experimental investigation on the mechanical performance of the Al2O3 and ZrO2 added Al-Mg-Si alloy for structural applications, Proc. Inst. Mech. Eng. Part E J. Process Mech. Eng. 238 (2023) 2223–2234. https://doi.org/10.1177/09544089231159777.

[12] J.J.M. Hillary, R. Ramamoorthi, J.D.J. Joseph, C.S.J. Samuel, A study on microstructural effect and mechanical behaviour of Al6061–5%SiC–TiB2 particulates reinforced hybrid metal matrix composites, J. Compos. Mater. 54 (2019) 2327–2337. https://doi.org/10.1177/0021998319894666.

[13] S.R. Oke, A. Bayode, O.E. Falodun, I.S. Olasupo, Microstructure, mechanical, and wear properties evaluation of Al-Cu based composite using RHA as reinforcement, Can. Metall. Q. (2023) 1–10. https://doi.org/10.1080/00084433.2024.2357859.

[14] M.O. Bodunrin, K.K. Alaneme, L.H. Chown, Aluminium matrix hybrid composites: a review of reinforcement philosophies; Mechanical, corrosion and tribological characteristics., J. Mater. Res. Technol. 4 (2015) 434–445. https://doi.org/10.1016/j.jmrt.2015.05.003.

[15] F. Ben, P.A. Olubambi, Agro waste reinforcement of metal matrix composites , a veritable sustainable engineering achievement , or an effort in futility ? A critical review Agro waste reinforcement of metal matrix composites , a veritable sustainable engineering achievement , or, Mater. Res. Express 11 (2024) 1–37. https://doi.org/10.1088/2053-1591/ad5642.

[16] A.A. Abdulrazaq, S. Ahmed, F.M. Mahdi, Agricultural waste and natural dolomite for green production of

aluminum composites, Clean. Eng. Technol. 12 (2023) 100588. https://doi.org/10.1016/j.clet.2022.100588.

[17] L. Osunmakinde, T.B. Asafa, P.O. Agboola, M.O. Durowoju, Development of aluminum composite reinforced with selected agricultural residues, Discov. Mater. 3 (2023). https://doi.org/10.1007/s43939-023-00069-z.

[18] K.K. Alaneme, I.B. Akintunde, P.A. Olubambi, T.M. Adewale, Fabrication characteristics and mechanical behaviour of rice husk ash - Alumina reinforced Al-Mg-Si alloy matrix hybrid composites, J. Mater. Res. Technol. 2 (2013) 60–67. https://doi.org/10.1016/j.jmrt.2013.03.012.

[19] S.P. Dwivedi, A.K. Srivastava, N.K. Maurya, R. Sahu, Microstructure and mechanical behaviour of Al/SiC/agro-waste RhA hybrid metal matrix composite, Rev. Des Compos. Des Mater. Av. 30 (2020) 43–47. https://doi.org/10.18280/rcma.300107.

[20] N.E. Udoye, G.E. Ezike, O.S.I. Fayomi, J.O. Dirisu, The Study on Mechanical and Electrical Properties of AA6061/Snail Shell Composites, Int. J. Chem. Eng. 2022 (2022) 1–9.

[21] F.O. Edoziuno, C.C. Nwaeju, A.A. Adediran, B.U. Odoni, V.R. Arun, Mechanical and microstructural characteristics of Aluminium 6063 Alloy / Palm Kernel shell composites for lightweight applications, Sci. African 12 (2021) 1–17. https://doi.org/10.1016/j.sciaf.2021.e00781.

[22] F. Ben, F.R. Amodu, P.A. Olubambi, Influence of Green Plantain Peel Ash and Alumina Reinforcement on the Physio-Mechanical Properties of Aluminium Matrix Hybrid Composites, in: Mater. Sci. Forum, 2023: pp. 33–45. https://doi.org/10.4028/p-5CdJMw.

[23] L. Purushothaman, P. Bala, MECHANICAL AND TRIBOLOGICAL BEHAVIOUR OF ALUMINIUM Al6061- COCONUT SHELL ASH COMPOSITE USING STIR CASTING PELLET METHOD, J. Balk. Tribol. Assoc. 22 (2016) 4008–4018.

[24] O. Olaniran, A. Oyetunji, B. Oji, Influence of Silicon Carbide-Cassava Peel Ash Weight Ratio on the Mechanical and Tribological Characteristics of Al-Mg-Si Alloy, J. Chem. Technol. Metall. 56 (2021) 1082–1088.

[25] L. Jaga, J.S. Vishwanatha, J.P. Ganjigatti, G. Irfan, R. Thara, Investigation of mechanical properties of Al6061 with reinforcement of coconut shell ash and graphene metal matrix composites, Mater. Today Proc. 92 (2023) 413–417. https://doi.org/10.1016/j.matpr.2023.05.529.

[26] J.E. Oghenevweta, V.S. Aigbodion, Mechanical properties and microstructural analysis of Al – Si – Mg / carbonized maize stalk waste particulate composites, J. King Saud Univ. - Eng. Sci. 28 (2016) 222–229. https://doi.org/10.1016/j.jksues.2014.03.009.

[27] O.O. Daramola, A.A. Adediran, A.T. Fadumiye, Evaluation of the mechanical properties and corrosion behaviour of coconut shell ash reinforced aluminium (6063) alloy composites, Leonardo Electron. J. Pract. Technol. 1 (2021) 107–119.

[28] B. Ufuoma, E. Francis, N. Cynthia, O. Richard, Experimental analysis , predictive modelling and optimization of some physical and mechanical properties of aluminium 6063 alloy based composites reinforced with corn cob ash ., J. Mater. Eng. Struct. 7 (2020) 451–465.

[29] A. Chaithanyasai, P. Rani, V. Umasankar, The microstructural and mechanical property study of effects of EGG SHELL particles on the Aluminum 6061, Procedia Eng. 97 (2014) 961–967. https://doi.org/10.1016/j.proeng.2014.12.372.

[30] K. Varalakshmi, K.C.K. Kumar, A.J. Babu, Analysis of dry sliding wear behaviour of al 6061-coconut shell ash metal matrix composites using stir casting, Appl. Eng. Lett. 4 (2019) 55–65. https://doi.org/10.18485/aeletters.2019.4.2.3.

[31] A. k. Virkunwar, S. Ghosh, R. Basak, Study of Mechanical and Tribological Characteristics of Aluminium Alloy Reinforced with Sugarcane Bagasse Ash, in: Int. Conf. Tribol. TRIBOINDIA-2018, 2019. https://doi.org/10.2139/ssrn.3313510.

[32] M.S. Kumar, A.A. Akinwande, C.-H. Yang, M. Vignesh, V. Romanovski, Investigation on mechanical behaviour of Al–Mg-Si alloy hybridized with calcined eggshell and TiO2 particulates, Biomass Convers. Biorefinery 14 (2024) 22215–22226. https://doi.org/10.1007/s13399-023-04215-8.

[33] F. Ben, Valorization of Manihot esculenta peel from environmental pollutant to sustainable engineering solutions for a cleaner future, Environ. Sci. Pollut. Res. 32 (2024) 1–27. https://doi.org/10.1007/s11356-024-35621-8.

[34] FAO, Crops and livestock products, 2023. https://www.fao.org/faostat/en/#data/QCL.

[35] U.G.. Eziefula, H.E. Opara, B.I. Eziefula, BEHAVIOUR OF CONCRETE CONTAINING CASSAVA PEEL ASH AS POZZOLAN, Umudike J. Eng. Technol. 5 (2019) 1–5. https://doi.org/10.33922/j.ujet_si1_6.

[36] S.B. Raheem, E.D. Arubike, O.S. Awogboro, Effects of Cassava Peel Ash (CPA) as Alternative Binder in Concrete, Int. J. Constr. Res. Civ. Eng. 1 (2020) 27–32.

[37] J. Ospino, J.P. Parra-Barraza, S. Cervera, E.E. Coral-Escobar, O.Á. Vargas-Ceballos, Activated carbon from cassava peel: a promising electrode material for supercapacitors, Rev. Fac. Ing. Univ. Antioquia (2020) 88–95. https://doi.org/10.17533/udea.redin.20200803.

[38] A.U. Ofoefule, E.O. Uzodinma, Biogas production from blends of cassava (Manihot utilissima) peels with some animal wastes, Int. J. Phys. Sci. 4 (2009) 398–402.

[39] UN-Energy, Achieving Universal Access by 2030 and Net-Zero Emissions By 2050: A Global Roadmap for Just and Inclusive Clean Cooking Transition., 2023. https://sdgs.un.org/sites/default/files/2023-07/UN-Energy Policy Brief - Clean Cooking Netzero pathway- 7-12-23 clean with cover page2_0.pdf.

[40] S. S, S.R. S, A. Nair, S. S, Investigation on mechanical properties of aluminum hybrid matrix composites reinforced with fly ash and titanium diboride using stir casting technique, Mater. Res. Express 11 (2024) 76523. https://doi.org/10.1088/2053-1591/ad6238.

[41] A.F. Owa, P.A. Olubambi, Development and Structural Evaluation of Dog Bone Particle – Reinforced Epoxy Composites for Biomedical Applications, Adv. Mater. Sci. Eng. 2024 (2024) 1–9. https://doi.org/10.1155/2024/2259630.

[42] A. Devi, S.S. Diarra, Factors Affecting the Utilisation of Cassava Products for Poultry Feeding [Review], Egypt. J. Vet. Sci. 52 (2021) 387–403.

[43] S. Leeson, J.D. Summers, Commercial Poultry Nutrition, Third Edit, Nottingham University Press, Nottingham, 2009.

[44] F. Ben, P.A. Olubambi, Synergistic effects of agro - waste ash and alumina on the surface texture and tribological properties of hybrid AMCs, Discov. Mater. 5 (2025) 23. https://doi.org/10.1007/s43939-025-00228-4.

[45] B. Festus, T. Ewetumo, K.D. Adedayo, S.S. Oluyamo, Development of a Low-Cost Thermal Heater-Cooler Blocks Using Locally Recycled Waste, J. Biosens. Bioelectron. 10 (2019) 1–4. https://www.hilarispublisher.com/open-access/development-of-a-lowcost-thermal-heatercooler-blocks-using-locally-recycled-waste.pdf (accessed October 29, 2024).

[46] ASTM D2734, Standard Test Methods for Void Content of Reinforced Plastics (ASTM D2734-23), 2023. https://doi.org/10.1520/D2734-23.2.

[47] H.J.P. Keighley, Archimedes' Principle and Flotation BT - Work Out Physics 'O' Level and GCSE, in: H.J.P. Keighley (Ed.), Macmillan Education UK, London, 1986: pp. 58–64. https://doi.org/10.1007/978-1-349-07213-2_6.

[48] ASTM-E10, Standard Test Method for Brinell Hardness of Metallic Materials (ASTM E10 — 23), 2023. https://doi.org/10.1520/E0010-23.

[49] B.J. Singh, R. Sehgal, Y.K. Singla, Chapter 5 Unleashing the essence of aluminum metal matrix composites through advanced characterization and mechanical analysis, in: G. Singh, R.P. Singh, N. Sharma, J.P. Davim (Eds.), Green Compos. Manuf., De Gruyter, 2024: pp. 105–132. https://doi.org/doi:10.1515/9783111067346-005.

[50] N. Saba, M. Jawaid, M.T.H. Sultan, An overview of mechanical and physical testing of composite materials, Elsevier Ltd, 2019. https://doi.org/10.1016/B978-0-08-102292-4.00001-1.

[51] ASTM-E8M, Standard Test Method for Tension Testing of Metallic Materials (Metric), in: Annu. B. ASTM Stand., Philadelphia, 1991.

[52] F. Versino, O. V López, M.A. García, Sustainable use of cassava (Manihot esculenta) roots as raw material for biocomposites development, Ind. Crops Prod. 65 (2015) 79–89. https://doi.org/10.1016/j.indcrop.2014.11.054.

[53] S. Mohd-asharuddin, N. Othman, M.Z. Nur Shaylinda, H.A. Tajarudin, A Chemical and Morphological Study of Cassava Peel: A Potential Waste as Coagulant Aid, in: MATEC Web Conf., 2017: pp. 1–8.

[54] T.F. Awolusi, O.J. Aladegboye, O.E. Babalola, E.K. Ayo, M. Azab, A.F. Deifalla, Optimizing the Flexural Behavior of Bamboo Reinforced Concrete Beams Containing Cassava Peel Ash using Response Surface Methodology, Civ. Eng. J. 9 (2023) 1971–1990.

[55] M.T. Abdulwahab, O.A.U. Uche, Durability Properties of Self-Compacting Concrete (SCC) Incorporating Cassava Peel Ash (CPA), Niger. J. Technol. 40 (2021) 584–590. https://doi.org/10.4314/njt.v40i4.4 Durability.

[56] E.B. Ogunbode, B.B. Nyakuma, R.A. Jimoh, T.A. Lawal, H.G. Nmadu, Mechanical and microstructure

properties of cassava peel ash–based kenaf bio-fibrous concrete composites, Biomass Convers. Biorefinery 13 (2023) 6515–6525. https://doi.org/10.1007/S13399-021-01588-6/FIGURES/10.

[57] J.A. Adebisi, J.O. Agunsoye, S.A. Bello, M. Haris, M.M. Ramakokovhu, M.O. Daramola, S.B. Hassan, Extraction of Silica from Cassava Periderm using Modified Sol-Gel Method, Niger. J. Technol. Dev. 15 (2016) 57–65. https://doi.org/10.4314/njtd.v15i2.4.

[58] J.M.N. Jayaweera, M. Narayana, S.U. Adikary, Effects of Kaolin with High Silica Content on Properties of Ceramic Tiles, in: 2022 Moratuwa Eng. Res. Conf., 2022: pp. 1–6. https://doi.org/10.1109/MERCon55799.2022.9906261.

[59] E. Kasai, Y. Sakano, T. Kawaguchi, T. Nakamura, Influence of Properties of Fluxing Materials on the Flow of Melt Formed in the Sintering Process, ISIJ Int. 40 (2000) 857–862. https://doi.org/10.2355/isijinternational.40.857.

[60] J.E. Zhou, K. Liu, W.X. Dong, Q.F. Bao, T.G. Zhao, Y.Q. Wang, Effects of CaO-Li2O-K2O-Na2O Fluxing Agents on the Properties of Porcelain Ceramic Tiles, Key Eng. Mater. 655 (2015) 258–262. https://doi.org/10.4028/www.scientific.net/KEM.655.258.

[61] C. Ogbonna, E.M. Mbadike, G.U. Alaneme, Effects of Cassava-Peel Ash on Mechanical Properties of Concrete, Umudike J. Eng. Technol. 6 (2020) 61–75. https://doi.org/10.33922/j.ujet_v6i2_8.

[62] Q. Xue, Y. He, X. Zhang, X. Zhang, M. Cai, C.F. Guo, C. Yang, Strong Interfaces Enable Efficient Load Transfer for Strong, Tough, and Impact-Resistant Hydrogel Composites, ACS Appl. Mater. Interfaces 14 (2022) 33797–33805. https://doi.org/10.1021/acsami.2c07133.

[63] Y. Hui, Y. Wang, X. Chen, X. Wang, Y. Gao, K. Wen, S. Cheng, J. Zhang, J. Shao, Synergistic enhancement of strength and toughness of fiber-reinforced composites by constructing biomimetic intermittent porous structure, Compos. Part A Appl. Sci. Manuf. 185 (2024) 108335. https://doi.org/10.1016/j.compositesa.2024.108335.

[64] G.S. Balan, S.A. Raj, Effect of thermal shocks on the interfacial bond strength of sandwich composites built with rigid and soft materials produced through extrusion process, Results Eng. 24 (2024) 103131. https://doi.org/10.1016/j.rineng.2024.103131.

[65] S. Sethi, B.C. Ray, Environmental effects on fibre reinforced polymeric composites: Evolving reasons and remarks on interfacial strength and stability, Adv. Colloid Interface Sci. 217 (2015) 43–67. https://doi.org/10.1016/j.cis.2014.12.005.

[66] V.S. Aigbodion, O.J. Agunsoye, R.O. Edokpia, I.C. Ezema, Performance Analysis of a Connecting Rod Produced with Al-Cu-Mg/Bean Pod Ash Nanoparticles., Silicon 10 (2018) 107-113. https://doi.org/10.1007/s12633-015-9382-8.

[67] H. Wakudkar, S. Mandal, A. Rani, S. Gangil, A. Das, Experimental investigations on valorization of corncob residues for synthesis of crystalline cellulose, Biomass Convers. Biorefinery (2025). https://doi.org/10.1007/s13399-025-06715-1.

[68] O.S. Olusesi, N.E. Udoye, Development and characterization of AA6061 aluminium alloy /clay and rice husk ash composite, Manuf. Lett. 29 (2021) 34–41. https://doi.org/10.1016/j.mfglet.2021.05.006.

[69] B. Festus, T. Ewetumo, S.S. Oluyamo, P.A. Olubambi, Characterization of Heater-Cooler Blocks Fabricated from Aluminium Wastes for Steady-State Thermal Application, Mater. Sci. Forum 1079 (2022) 147–155. https://doi.org/10.4028/p-s7wbe2.

[70] A.M. Razzaq, D.L.A. Abdul Majid, M.R. Ishak, U. M. B, A Brief Research Review for Improvement Methods the Wettability between Ceramic Reinforcement Particulate and Aluminium Matrix Composites, IOP Conf. Ser. Mater. Sci. Eng. 203 (2017) 12002. https://doi.org/10.1088/1757-899X/203/1/012002.

[71] M. Malaki, A.F. Tehrani, B. Niroumand, A. Abdullah, Ultrasonically Stir Cast SiO2/A356 Metal Matrix Nanocomposites, Metals (Basel). 11 (2021). https://doi.org/10.3390/met11122004.

[72] N.K. Votarikari, N. Kishore Nath, P. Ramesh Babu, Evaluating and Optimising Tribological Parameters of Enhanced Two-Step Stir Cast Al6061/Nano-SiO2 Composite Using Machine Learning Techniques, J. Bio- Tribo-Corrosion 10 (2024) 66. https://doi.org/10.1007/s40735-024-00873-x.

[73] A.R.R. Kaladgi, K. Fazlur Rehman, A. Afzal, M.A. Baig, M.E.M. Soudagar, S. Bhattacharyya, Fabrication characteristics and mechanical behaviour of aluminium alloy reinforced with Al2O3 and coconut shell particles synthesized by stir casting, IOP Conf. Ser. Mater. Sci. Eng. 1057 (2021) 1–15. https://doi.org/10.1088/1757-899x/1057/1/012017.

[74] R.N. Muni, J. Singh, V. Kumar, S. Sharma, Influence of rice husk ash, cu, mg on the mechanical behaviour of aluminium matrix hybrid composites, Int. J. Appl. Eng. Res. 14 (2019) 1828–1834.

[75] K.K. Alaneme, K.O. Sanusi, Microstructural characteristics, mechanical and wear behaviour of aluminium matrix hybrid composites reinforced with alumina, rice husk ash and graphite, Eng. Sci. Technol. an Int. J. 18 (2015) 416–422. https://doi.org/10.1016/j.jestch.2015.02.003.

[76] K.E. Aifantis, J.R. Willis, The role of interfaces in enhancing the yield strength of composites and polycrystals, J. Mech. Phys. Solids 53 (2005) 1047–1070. https://doi.org/10.1016/j.jmps.2004.12.003.

[77] J. Chen, Q. Hui, C. Li, X. Li, D. Shao, N. Cheng, Effects of Interfacial Features on Yield Strength of Particle Reinforced Metal Matrix Composites, MATEC Web Conf. 67 (2016). https://doi.org/10.1051/matecconf/20166706015.

[78] Z. Zhang, D.L. Chen, Consideration of Orowan strengthening effect in particulate-reinforced metal matrix nanocomposites : A model for predicting their yield strength, Scr. Mater. 54 (2006) 1321–1326. https://doi.org/10.1016/j.scriptamat.2005.12.017.

[79] J. Chen, Y. Han, S. Li, Z. Wei, J. Le, H. Shi, G. Huang, W. Lu, D. Zhang, Evading the strength and ductility trade-off dilemma in titanium matrix composites through designing bimodal grains and micro-nano reinforcements, Scr. Mater. 235 (2023) 115625. https://doi.org/10.1016/j.scriptamat.2023.115625.

[80] Z.Y. Xu, C.F. Fang, N. Wang, R. Wang, X.P. Zhang, Y.M. Wang, Overcoming the strength-ductility trade-off of an AZ31 matrix composite reinforced by in-situ spherical Al3Fe nanoparticles, Compos. Part B Eng. 242 (2022) 110069. https://doi.org/10.1016/j.compositesb.2022.110069.

[81] B. Parveez, A. Maleque, Influence of agro-based reinforcements on the properties of aluminum matrix composites: a systematic review, J. Mater. Sci. 56 (2021) 16195–16222. https://doi.org/10.1007/s10853-021-06305-2.

[82] X. Zhang, T. Chen, S. Ma, H. Qin, J. Ma, Overcoming the strength-ductility trade-off of an aluminum matrix composite by novel core-shell structured reinforcing particulates, Compos. Part B Eng. 206 (2021) 108541. https://doi.org/10.1016/j.compositesb.2020.108541.

[83] Z. Yang, G. Kang, R. Liu, P. Chen, Effect of particle morphology on mechanical behaviour of highly particle-filled composites, Int. J. Mech. Sci. 227 (2022) 107446. https://doi.org/10.1016/j.ijmecsci.2022.107446.

[84] L. Osunmakinde, T.B. Asafa, P.O. Agboola, M.O. Durowoju, A Systemic review of the influence of eco-friendly particles on hybrid composites synthesized via stir casting technique, Discov. Mech. Eng. 3 (2024). https://doi.org/10.1007/s44245-024-00055-6.

[85] K. Alaneme, A. Aluko, Fracture toughness (K1C) and tensile properties of as-cast and age-hardened aluminium (6063) – silicon carbide particulate composites., Sci Iran 19 (2012) 992–6.

[86] G. Chakravarthi, K. Giridharan, S.M. Kumar, N.S. Sivakumar, Enhancement of mechanical, microstructural and fatigue properties of cassava tuber peel biosilica toughened dissimilar AA 6061-AZ31B Mg welds, Polym. Bull. (2025). https://doi.org/10.1007/s00289-025-05732-4.

[87] V. V. Ganesh, N. Chawla, Effect of particle orientation anisotropy on the tensile behavior of metal matrix composites: Experiments and microstructure-based simulation, Mater. Sci. Eng. A 391 (2005) 342–353. https://doi.org/10.1016/j.msea.2004.09.017.

[88] H. Zhang, M.W. Chen, K.T. Ramesh, J. Ye, J.M. Schoenung, E.S.C. Chin, Tensile behavior and dynamic failure of aluminum 6092/B4C composites, Mater. Sci. Eng. A 433 (2006) 70–82. https://doi.org/10.1016/j.msea.2006.06.055.